



**HAL**  
open science

## Tuning the high temperature properties of PrSrCoO<sub>4</sub> cathode with Cu<sup>2+</sup> dopant for intermediate temperature solid oxide fuel cells

Jian-Wei Liu, Qiang Li, Li-Ping Sun, Li-Hua Huo, Hui Zhao, Jean-Marc. Bassat, Sébastien Fourcade, Jean-Claude Grenier

► **To cite this version:**

Jian-Wei Liu, Qiang Li, Li-Ping Sun, Li-Hua Huo, Hui Zhao, et al.. Tuning the high temperature properties of PrSrCoO<sub>4</sub> cathode with Cu<sup>2+</sup> dopant for intermediate temperature solid oxide fuel cells. *Renewable Energy*, 2020, 159, pp.486-493. 10.1016/j.renene.2020.06.032 . hal-02885979

**HAL Id: hal-02885979**

**<https://hal.science/hal-02885979>**

Submitted on 9 Jul 2020

**HAL** is a multi-disciplinary open access archive for the deposit and dissemination of scientific research documents, whether they are published or not. The documents may come from teaching and research institutions in France or abroad, or from public or private research centers.

L'archive ouverte pluridisciplinaire **HAL**, est destinée au dépôt et à la diffusion de documents scientifiques de niveau recherche, publiés ou non, émanant des établissements d'enseignement et de recherche français ou étrangers, des laboratoires publics ou privés.

1     **Tuning the high temperature properties of PrSrCoO<sub>4</sub> cathode with**  
2     **Cu<sup>2+</sup> dopant for intermediate temperature solid oxide fuel cells**

3     Liu Jian-Wei <sup>a</sup>, Li Qiang <sup>a</sup>, Sun Li-Ping <sup>a,\*</sup>, Huo Li-Hua <sup>a</sup>, Zhao Hui <sup>a,\*</sup>, Jean-Marc  
4     Bassat <sup>b</sup>, Sébastien Fourcade <sup>b</sup>, Jean-Claude Grenier <sup>b</sup>

5  
6     <sup>a</sup> *Key Laboratory of Functional Inorganic Material Chemistry, Ministry of Education,*  
7     *School of Chemistry and Materials Science, Heilongjiang University, Harbin 150080*  
8     *P. R. China*

9     <sup>b</sup> *CNRS, Université de Bordeaux, ICMCB, 87 avenue du Dr. A. Schweitzer, F-33608*  
10    *Pessac-Cedex, France*

11    **Abstract**

12    PrSrCo<sub>1-x</sub>Cu<sub>x</sub>O<sub>4+δ</sub> ( $x = 0.0, 0.1, 0.3, 0.5$ ) are synthesized by solid-state reaction  
13    method. The effects of Cu<sup>2+</sup> doping on electrical conductivity, thermal expansion,  
14    oxygen diffusion properties and oxygen reduction reaction (ORR) activity are  
15    investigated. PrSrCo<sub>1-x</sub>Cu<sub>x</sub>O<sub>4+δ</sub> oxides crystallize in a single-phase tetragonal  
16    structure with *I4/mmm* space group. Partial substitution Co<sup>3+</sup> by Cu<sup>2+</sup> results the  
17    increase of electrical conductivity and decrease of thermal expansion coefficient.  
18    Introducing Cu<sup>2+</sup> promotes the formation of interstitial oxygen, accelerates the  
19    kinetics of oxygen transport, and significantly improves the electrocatalytic activity of

---

Corresponding author. Tel.: +86 45186608426; fax: +86 45186608426.

E-mail address: sunliping@hlju.edu.cn (L-P. Sun), zhaohui98@hlju.edu.cn (H. Zhao)

1 ORR. The lowest area specific resistance (ASR) value of  $0.08 \Omega \text{ cm}^2$  is obtained for  
2 the  $\text{PrSrCo}_{0.7}\text{Cu}_{0.3}\text{O}_{4+\delta}$  cathode at  $700 \text{ }^\circ\text{C}$  in air. The ORR mechanism study  
3 demonstrates that Cu-doping (30 %) promotes the charge transfer process. The  
4 reaction rate control step on  $\text{PrSrCo}_{0.7}\text{Cu}_{0.3}\text{O}_{4+\delta}$  cathode is the dissociation and surface  
5 diffusion process of adsorbed molecular oxygen.

6 **Keywords:** solid oxide fuel cells (SOFCs);  $\text{K}_2\text{NiF}_4$  structure; cathode material;  
7 electrochemical properties

8

## 9 **1. Introduction**

10 The  $\text{A}_2\text{BO}_4$  oxides with  $\text{K}_2\text{NiF}_4$ -type structure have been considered as promising  
11 cathode materials for intermediate temperature solid oxide fuel cells (IT-SOFCs), due  
12 to their high oxygen diffusion and exchange coefficients, good electronic conductivity,  
13 suitable thermal expansion coefficient (TEC) for typical electrolytes and excellent  
14 electrocatalytic activity towards oxygen reduction reaction (ORR) [1-4].  $\text{A}_2\text{BO}_4$   
15 oxides can be considered as a superstructure that composed by perovskite layer  
16 ( $\text{ABO}_3$ ) and rock salt layer (AO) alternatively overlapped along c-axis direction. Due  
17 to the insertion character of rock salt layer, these materials exhibit special structural  
18 flexibility: they can withstand reducing conditions via loss of oxygen, usually from  
19 equatorial planes, and accommodate excess interstitial oxygen under oxidizing  
20 conditions [5]. Studies have proved that the presence of rock salt block in T-phase  
21  $\text{A}_2\text{BO}_4$  favors the high oxygen mobility in the bulk material [6]. Compared to the  
22 traditional  $\text{ABO}_3$  perovskite oxides, these  $\text{A}_2\text{BO}_4$  materials show relatively large

1 oxygen ion conductivity and promising electrode performance. Therefore, Nickelate  
2 and copper based  $A_2BO_4$  oxides with mixed ionic-electronic conducting (MIEC)  
3 properties have been thoroughly evaluated as cathode materials for IT-SOFCs [7-20].  
4 In contrast to the wealth of data accumulated on nickelate and copper oxides, few  
5 studies have been reported to date on the structure and electrochemical catalytic  
6 activity of cobalt-based  $A_2BO_4$  oxides. An early study in 2005 by Munnings et al.  
7 found that the oxygen diffusion coefficient ( $D^*$ ) and oxygen exchange coefficient ( $k^*$ )  
8 of  $La_2CoO_{4+\delta}$  were even higher than that of  $La_2NiO_{4+\delta}$  at  $T < 700$  °C [21]. Wang and  
9 Nie reported that  $Ln_2CoO_4$  ( $Ln=Pr$  and  $Sm$ ) could be applied as cathodes for SOFC  
10 via studying their thermal stability and conductive properties [22]. The  
11 electrochemical properties of Co-based  $A_2BO_4$  materials can be further optimized by  
12 doping aliovalent elements in A and/or B site. For instance, the transport properties of  
13  $Sr^{2+}$  doped  $La_{2-x}Sr_xCoO_{4+\delta}$  have been systematically investigated [23]. In another  
14 study, the effects of Sb doping on the cathode property of  $LaSrCo_{1-x}Sb_xO_4$  was  
15 reported by Wang et al [24]. Recently, Cao Y et al. evaluated the cathode performance  
16 of  $Pr_{2-x}Sr_xCoO_{4+\delta}$  materials. They found that  $Pr_{0.8}Sr_{1.2}CoO_{4+\delta}$  had the minimum  
17 polarization resistance of  $0.29 \Omega \cdot cm^2$  at  $700$  °C [25]. It was reported that  $ABO_3$   
18 perovskite with  $Cu^{2+}$  at B site always exhibited low TECs [26, 27], whereas Pr based  
19 perovskite oxides are known to exhibit high electrochemical activity, due to the redox  
20 cycles of  $Pr^{3+}$  cations in the lattice [28-30]. In this study,  $Cu^{2+}$  doped  
21  $PrSrCo_{1-x}Cu_xO_{4+\delta}$  are synthesized and the effects of  $Cu^{2+}$  substitution on the crystal

1 structure, high-temperature electrical conductivity, thermal expansion behavior and  
2 the electrochemical properties of the compounds are investigated. We propose the  
3  $\text{PrSrCo}_{1-x}\text{Cu}_x\text{O}_{4+\delta}$  material, which combine the merits of both  $\text{Cu}^{2+}$  dopants and  $\text{Pr}^{3+}$   
4 cations, would be potential cathode candidate for IT-SOFCs.

## 5 **2. Experimental**

### 6 2.1 Materials synthesis

7  $\text{PrSrCo}_{1-x}\text{Cu}_x\text{O}_{4+\delta}$  ( $x = 0.0, 0.1, 0.3, 0.5$ ) oxides are synthesized by traditional  
8 solid-state reaction method. The reactants are  $\text{Pr}_6\text{O}_{11}$ ,  $\text{SrCO}_3$ ,  $\text{Co}_3\text{O}_4$  and  $\text{CuO}$ . All of  
9 these materials are high purity (99.99, Aladdin industrial corporation, China), and  
10 used as received. According to the chemical formula, stoichiometric amount of above  
11 mentioned materials are mixed with ethanol in a planetary ball-mill for 1 h. Then the  
12 obtained mixtures are pressed into pellets under 100 MPa and reacted at 1000 °C for  
13 12 h in air. The obtained pellets are ground, tableted and reacted again at 1000 °C for  
14 additional 12 h. This operation is repeated three times until the target products are  
15 obtained. For thermal expansion coefficient (TEC) and electrical conductivity  
16 measurements, the product powders are pressed under 100 MPa and then sintered at  
17 1050 °C for 12 h in air, to form rectangular bars with dimensions 15 mm × 3 mm × 1  
18 mm. The relative bulk densities of the rectangular bars are over 95% of the theoretical  
19 values that measured by Archimedes method (Sartorius balance with a density kit).

### 20 2.2 Cell fabrication

21  $\text{Ce}_{0.9}\text{Gd}_{0.1}\text{O}_{1.95}$  (GDC) powder was obtained from Ningbo SuoFuRen Energy Co. Ltd.

1 (China). The GDC powders are pressed uniaxially at 220 MPa and then sintered at  
2 1400°C for 10 h to form dense pellet with 10 mm in diameter and 0.8mm in thickness.  
3 The cathode ink is prepared by mixing 100 mg  $\text{PrSrCo}_{1-x}\text{Cu}_x\text{O}_{4+\delta}$  powders with 4 mL  
4 terpineol containing 4% ethyl cellulose. The symmetric cell  $\text{PrSrCo}_{1-x}\text{Cu}_x\text{O}_{4+\delta}/\text{GDC}/$   
5  $\text{PrSrCo}_{1-x}\text{Cu}_x\text{O}_{4+\delta}$  is fabricated by painting the cathode ink on both sides of GDC  
6 pellet in symmetric configuration. The effective cathode area is 0.25 cm<sup>2</sup>. The cells  
7 are initially heated at 500 °C for 0.5 h to eliminate the organic binders, and then  
8 followed by calcinations at 950 °C for 3 h with a heating/cooling rate of 5 °C min<sup>-1</sup>.

9 The electrolyte-supported single cell Ni-GDC|GDC|  $\text{PrSrCo}_{0.7}\text{Cu}_{0.3}\text{O}_{4+\delta}$  is prepared  
10 for full cell performance test. NiO-GDC anode ink (NiO:GDC = 60:40 wt.%) is firstly  
11 painted on one side of GDC pellet, followed by heat-treatment at 1250 °C for 4 h in  
12 air to form anode with surface area of 0.25 cm<sup>2</sup>.  $\text{PrSrCo}_{0.7}\text{Cu}_{0.3}\text{O}_{4+\delta}$  cathode is then  
13 prepared on the other side of GDC pellet in symmetrical configuration.

### 14 2.3 Characterization

15 The phase purity and chemical compatibility of  $\text{PrSrCo}_{1-x}\text{Cu}_x\text{O}_{4+\delta}$  with GDC are  
16 characterized by powder X-ray diffraction method (XRD, Bruker AXS D8). The  
17 measurements are conducted at 40 kV and 40 mA using Cu  $K\alpha$  radiation. The  
18 diffraction data is collected in the  $2\theta$  range of 20°-75° with scanning speed 8°/min.  
19 The unit cell parameters are analyzed by LeBail refinement method with the Fullprof  
20 package. In the refinement procedure, the 6-coefficients polynomial function and  
21 Pseudo-Voigt function are selected to fit the background and peak shape, respectively.

1 TG measurements are performed from 25 °C to 900 °C in air, with the heating rate of  
2 10 °C/min using Setaram Setsys 16/18 thermoanalyser. The thermal expansion  
3 behavior of the sample is monitored in air from 100 °C to 800 °C with the heating rate  
4 of 5 °C/min (Setaram Setsys 16/18 dilatometer).

5 X-ray photoelectron spectroscopy (XPS) is recorded to study the surface oxygen  
6 species of the material. The measurement is performed using a Kratos Axis Ultra Dld  
7 photoelectron spectrometer equipped with Al K<sub>α</sub> (1486.6 eV) radiation source. The  
8 microstructure of the symmetrical cell is recorded using field-emission scanning  
9 electron microscope (FE-SEM, S-4800, Hitachi).

10 The electrical conductivity and electrical conductivity relaxation (ECR) of the  
11 specimens are measured by standard four-probe DC method. The conductivities are  
12 measured in the temperature range of 100-800 °C in air. The ECR measurements are  
13 performed at 650°C, 700°C and 750°C. In order to obtain the transient curve at each  
14 temperature, the oxygen partial pressure of the measurement atmosphere is switched  
15 rapidly from 20% to 2%.

16 The EIS diagrams are collected with electrochemical workstation (AUTOLAB,  
17 PGStat 30) under open circuit voltage (OCV). The applied frequency is ranged from  
18 1MHz to 0.01Hz, and the signal amplitude is 50 mV. The measurements are  
19 performed as a function of temperature (500 °C-700 °C) and oxygen partial pressure  
20 that controlled by N<sub>2</sub> (99.999%)/O<sub>2</sub> (99.999%) mixed atmosphere.

21 The power output performance of the electrolyte-supported single cell is tested with

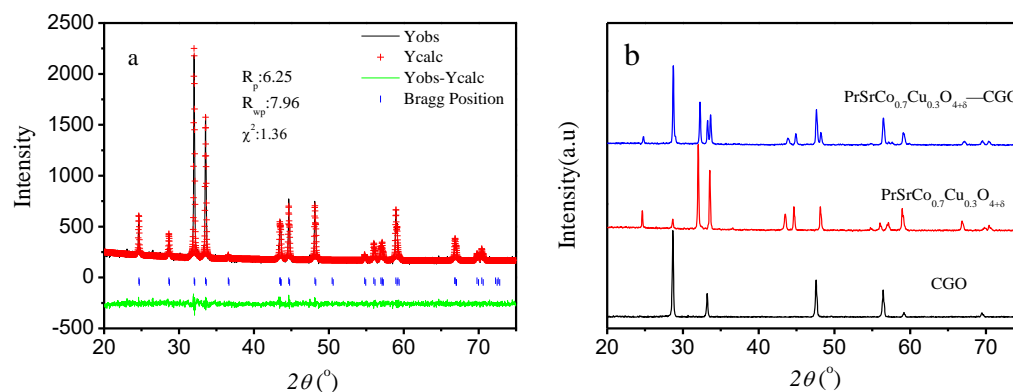
1 the device of ProboStat30. Humidified H<sub>2</sub> (97% H<sub>2</sub>/3% H<sub>2</sub>O) is fed to the anode  
2 chamber at a flow rate of 50 ml min<sup>-1</sup>, while the cathode is exposed to ambient air. Ag  
3 meshes are used as current collectors for both anode and cathode sides.

### 4 **3. Results and discussions**

#### 5 3.1 Phase identification

6 The XRD patterns of PrSrCo<sub>0.7</sub>Cu<sub>0.3</sub>O<sub>4+δ</sub> are shown in Figure 1a. All the patterns are  
7 similar to the reported PrSrCoO<sub>4</sub> material [31], indicating the sample is crystallized in  
8 single-phase K<sub>2</sub>NiF<sub>4</sub>-type structure with SG I4/mmm. The refinement results of the  
9 unit cell parameters are listed in Table 1. It is observed that the cell parameter c  
10 increases steadily with Cu<sup>2+</sup> doping. This observation can be understood, considering  
11 the Jahn-Teller effect of Cu<sup>2+</sup> with electronic configuration of d<sup>9</sup>. Cu<sup>2+</sup> cations tend to  
12 form square planar coordination. In this sense, the apical Cu–O distance is much  
13 longer than that of equatorial Cu–O distance in [CuO<sub>6</sub>] octahedron. In addition, more  
14 interstitial oxygen is generated in the rock-salt layer with Cu<sup>2+</sup> doping, which also  
15 causes the expansion of c-axis. The similar conclusions have been drawn in the other  
16 Cu<sup>2+</sup> doped Ln<sub>2</sub>NiO<sub>4</sub> materials [32-35]. On the other hand, the cell parameters a (b)  
17 decrease first and then increase again with the Cu<sup>2+</sup> doping, with an inflection point at  
18 x = 0.3. In order to maintain the charge neutrality requirement, Cu<sup>2+</sup> doping leads to  
19 the partial oxidation of Co<sup>3+</sup> to Co<sup>4+</sup>. According to the valence bond theory, the  
20 cobalt-oxygen bond is strengthened and the bond length along a(b)-axis direction  
21 decreases with the Cu<sup>2+</sup> doping. At the same time, we should also consider the size

1 effects of doped  $\text{Cu}^{2+}$  (the radius of  $\text{Cu}^{2+}$  (72 pm) is larger than that of  $\text{Co}^{3+}$  (63 pm)  
 2 and  $\text{Co}^{4+}$  (53 pm)). Therefore, the variation of cell parameters a (b) for  
 3  $\text{PrSrCo}_{1-x}\text{Cu}_x\text{O}_{4+\delta}$  oxides seems to be a competitive results of the doped amount of



4  
 5 Fig. 1. Experimental (black continuous line) and calculated (red line) XRD patterns,  
 6 and their difference (green line at the bottom) for  $\text{PrSrCo}_{0.7}\text{Cu}_{0.3}\text{O}_{4+\delta}$ . Blue vertical bar  
 7 indicate the position of Bragg peaks of the phases contained in the sample (a),  
 8 Mixture of  $\text{PrSrCo}_{0.7}\text{Cu}_{0.3}\text{O}_{4+\delta}$  with GDC after annealed at 1000 °C for 24 h in air (b).

9 **Table 1**

10 Cell parameters of  $\text{PrSrCo}_{1-x}\text{Cu}_x\text{O}_{4+\delta}$  ( $x = 0.0, 0.1, 0.3, 0.5$ ).

	$a/b$ (Å)	$c$ (Å)	$V$ (Å <sup>3</sup> )	Space group	$R_p$ (%)	$R_{wp}$ (%)	$\chi^2$
$\text{PrSrCoO}_{4+\delta}$							2.40
	3.792(3)	12.460(3)	179.19	$I4/mmm$	6.59	8.74	
$\text{PrSrCo}_{0.9}\text{Cu}_{0.1}\text{O}_{4+\delta}$							1.36
	3.790(2)	12.461(3)	179.01	$I4/mmm$	4.01	5.58	
$\text{PrSrCo}_{0.7}\text{Cu}_{0.3}\text{O}_{4+\delta}$							1.36
	3.781(3)	12.478(7)	178.39	$I4/mmm$	6.25	7.96	
$\text{PrSrCo}_{0.5}\text{Cu}_{0.5}\text{O}_{4+\delta}$							1.7
	3.787(6)	12.519(5)	179.55	$I4/mmm$	5.69	6.73	
							1

11  $\text{Cu}^{2+}$  and the valence state of Co ions. To assess the possible reaction between

1 PrSrCo<sub>0.7</sub>Cu<sub>0.3</sub>O<sub>4+δ</sub> and GDC electrolyte, the two oxide powders are mixed in weight  
2 ratio of 1:1, and then sintered at 1000 °C for 24 h in air. The XRD patterns of the  
3 sintered mixtures are shown in Fig. 1b. No additional peaks indicating new phase  
4 formation are detected from the patterns of the mixture. It is concluded that  
5 PrSrCo<sub>0.7</sub>Cu<sub>0.3</sub>O<sub>4+δ</sub> is chemically compatible with GDC below 1000 °C.

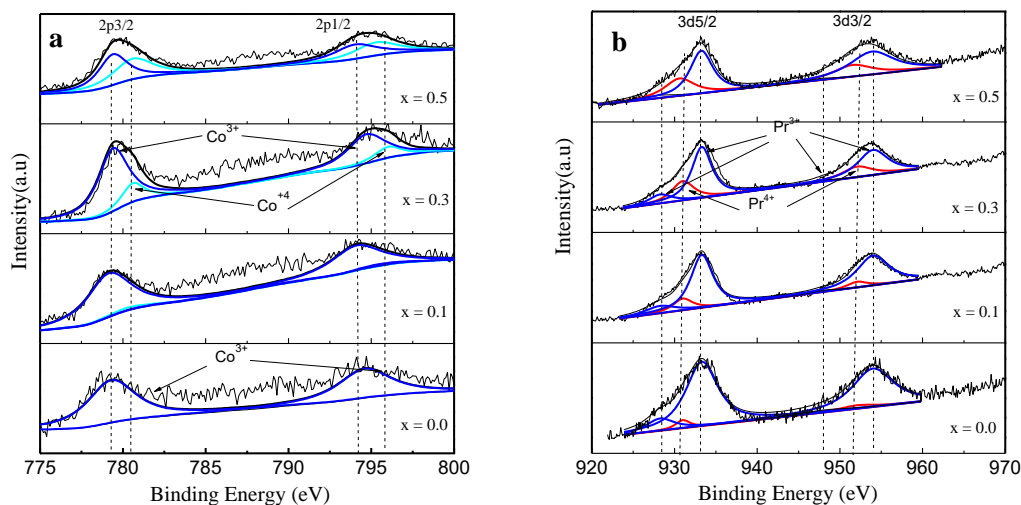
### 6 3.2 X-ray photoelectron spectroscopy analysis and Oxygen non-stoichiometry in 7 PrSrCo<sub>1-x</sub>Cu<sub>x</sub>O<sub>4+δ</sub>

8 To identify the surface properties of PrSrCo<sub>1-x</sub>Cu<sub>x</sub>O<sub>4+δ</sub> ( $x = 0.0, 0.1, 0.3, 0.5$ ) oxides,  
9 the chemical states of elemental Co, Cu, and O are measured by X-ray photoelectron  
10 spectroscopy (XPS) and normalized with C 1s peak at 284.6 eV. The strontium ions  
11 and copper ions exhibit mono-oxidation state as Sr<sup>2+</sup> and Cu<sup>2+</sup> in PrSrCo<sub>1-x</sub>Cu<sub>x</sub>O<sub>4+δ</sub>,  
12 while Pr and Co cations display mixed valance states. The Co 2p XPS spectra and the  
13 fitting curves are presented in Figure 2a. The peaks at 779.5 and 794.3 eV can be  
14 assigned to Co<sup>3+</sup> 2p<sub>3/2</sub> and 2p<sub>1/2</sub>, whereas the other set of peaks with binding energies  
15 of 780.8 and 795.5 eV represent Co<sup>4+</sup> 2p<sub>3/2</sub> and 2p<sub>1/2</sub>, respectively [36,37].

16 The Pr 3d XPS spectra and the fitting curves are presented in Figure 2b. The peaks  
17 with binding energy at 927.9/933.0 eV and 948.4/953.6 eV originate from Pr<sup>3+</sup> 3d<sub>5/2</sub>  
18 and 3d<sub>3/2</sub>, and the doublet peaks located at 931.0 eV and 952.3 eV can be assigned to  
19 Pr<sup>4+</sup> 3d<sub>5/2</sub> and 3d<sub>3/2</sub>, respectively [37,38]. The fitting results indicate that Pr<sup>3+</sup> coexists  
20 with Pr<sup>4+</sup> in these samples.

21 From the XPS analysis, the percentage contributions of different valence states are

1 calculated and the average valences of Pr and Co ions are tabulated in Table 2.



2  
3 Fig. 2. XPS spectra and fitting lines of Co 2p (a), Pr 3d (b) in  $\text{PrSrCo}_{1-x}\text{Cu}_x\text{O}_{4+\delta}$   
4 samples at room temperature.

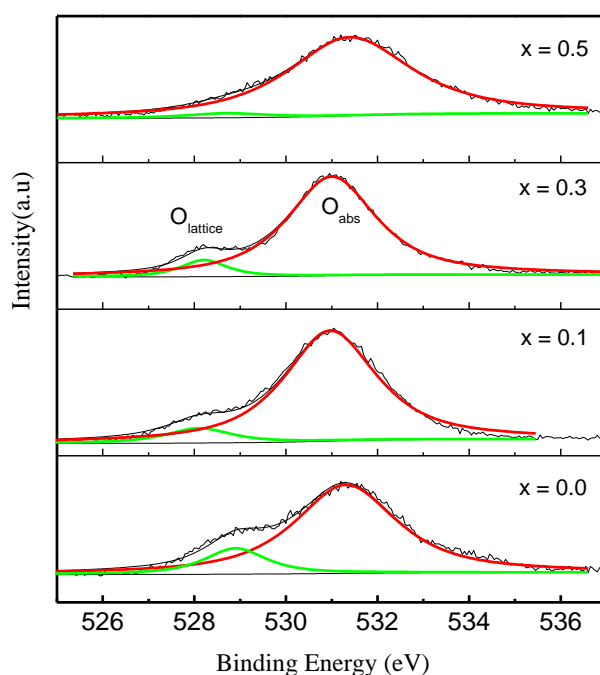
5 **Table 2**

6 Contents of non-stoichiometric oxygen ( $\delta$ ), average valences of Pr ( $m+$ ) and Co ( $n+$ )  
7 ions in  $\text{PrSrCo}_{1-x}\text{Cu}_x\text{O}_{4+\delta}$  oxides.

x	Pr <sup>m+</sup>	Co <sup>n+</sup>	$\delta$
0.0	3.04	3.00	0.02
0.1	3.11	3.06	0.03
0.3	3.26	3.23	0.06
0.5	3.42	3.49	0.08

8 Quantitative analysis of O content for each sample is carried out according to the XPS  
9 spectra and the results are also listed in Table 2. The oxygen contents for all of the  
10 as-prepared samples are found to be slightly above 4.0, indicating the existence of  
11 interstitial oxygen in the material. The average valences of Pr and Co increase steadily

1 with the substitution of Cu from  $x = 0.1$  to  $x = 0.5$ , and the overstoichiometric oxygen  
2 content ( $\delta$ ) increases from 0.02 to 0.08.  
3 Since oxygen species on the cathode surface play a key role for oxygen reduction  
4 reaction, the O1s XPS spectra of  $\text{PrSrCo}_{1-x}\text{Cu}_x\text{O}_{4+\delta}$  are further analyzed, and the  
5 fitting results are presented in Figure 3. The peak around  $528.5 \pm 0.4$  eV corresponds to  
6 the lattice oxygen ( $\text{O}_{\text{lattice}}$ ) associating to the redox properties of metal ions [24, 39-43].  
7 The broad peak centered around  $531.2 \pm 0.3$  eV can be assigned to the absorbed  
8 oxygen species ( $\text{O}_{\text{abs}}$ ) on surface [38-43].



9  
10 Fig. 3. O 1s core-level spectra and fitting lines of  $\text{PrSrCo}_{1-x}\text{Cu}_x\text{O}_{4+\delta}$  at room  
11 temperature.  
12 Table 3 summarizes the area percentage of different kinds of oxygen species in  
13  $\text{PrSrCo}_{1-x}\text{Cu}_x\text{O}_{4+\delta}$ . Obviously, the amount of chemisorbed oxygen increases with the

1 value of  $x$ , implying the improved ORR catalytic activity of  $\text{Cu}^{2+}$  doped materials.

2 **Table3**

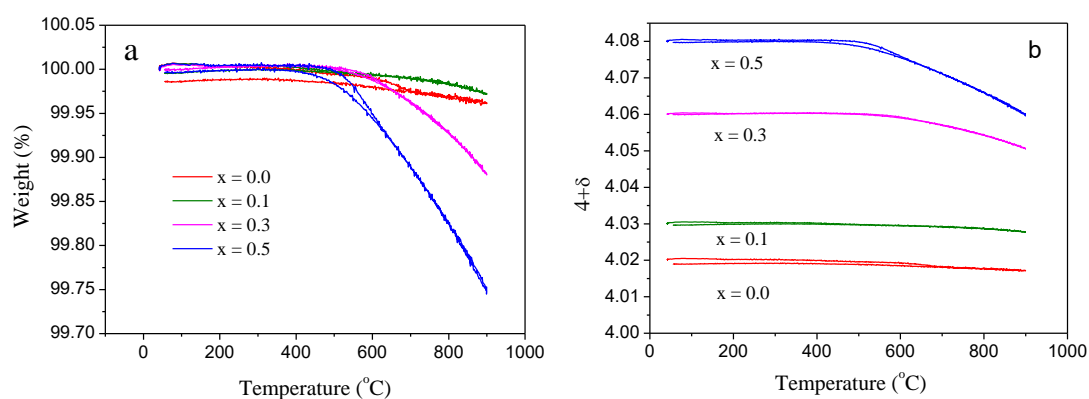
3 The fitting results of O 1s XPS spectra for  $\text{PrSrCo}_{1-x}\text{Cu}_x\text{O}_{4+\delta}$ .

$\text{PrSrCo}_{1-x}\text{Cu}_x\text{O}_{4+\delta}$	$\text{O}_{\text{lattice}}$		$\text{O}_{\text{abs}}$	
	Position(eV)	Area(%)	Position(eV)	Area(%)
$x = 0.0$	528.9	14.9	531.3	85.1
$x = 0.1$	528.1	8.7	530.9	91.3
$x = 0.3$	528.2	8.0	531.0	92.0
$x = 0.5$	528.7	3.6	531.4	96.4

4 3.3 Surface oxygen exchange and Electrical conductivity relaxation

5 It is known that the lattice oxygen in the perovskite oxides can be released at high  
6 temperatures and leads to changes of the point defects. To get this knowledge, the  
7 thermogravimetric analysis (TGA) is performed on  $\text{PrSrCo}_{1-x}\text{Cu}_x\text{O}_{4+\delta}$  samples (Figure  
8 4a). The measurement is carried out within two consecutive thermo-cycles in between  
9 room temperature up to 900 °C with a ramp of 10 °C  $\text{min}^{-1}$  each cycle, and the data of  
10 the second cycle is recorded. The corresponding oxygen non-stoichiometry as a  
11 function of temperature is determined from the weight change of the sample,  
12 assuming the initial oxygen content is obtained from the XPS analysis (Figure 4b). All  
13 the samples show weight loss at temperatures above  $\sim 400$  °C, due to the  
14 thermal-driven release of interstitial oxygen from the lattice, accompanied by the  
15 reduction of Co ions. It can be observed that the weight loss of the samples with  $x =$

1 0.0 and 0.1 are very small, while it becomes significant for the samples with  $x = 0.3$   
 2 and 0.5. In addition, the  $\text{Cu}^{2+}$  doped materials exhibit reversible behavior of oxygen  
 3 lose and uptake throughout the heating/cooling cycles.

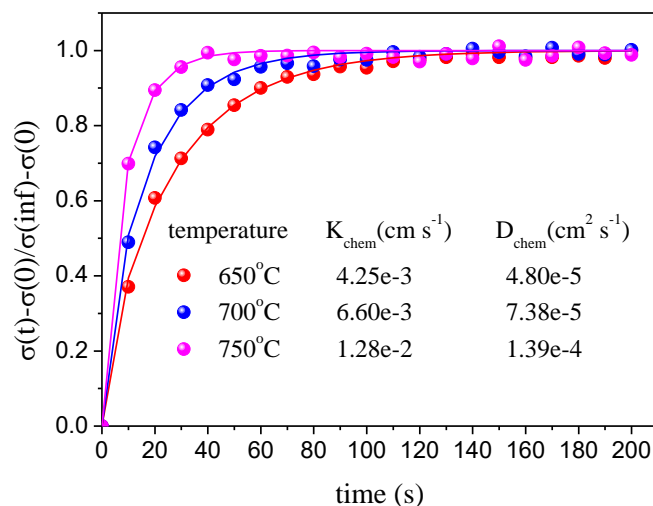


4  
 5 Fig. 4. (a) Thermogravimetric curves of  $\text{PrSrCo}_{1-x}\text{Cu}_x\text{O}_{4+\delta}$  ( $x = 0.0 \sim 0.5$ ); (b)  
 6 corresponding oxygen non-stoichiometry plots as function of temperatures.

7 For  $\text{PrSrCoO}_{4+\delta}$  however, the weight could not reach to its initial value after the  
 8 thermo-cycle. This behavior suggests that the oxygen exchange process between the  
 9 oxides and gaseous oxygen is promoted for the  $\text{Cu}^{2+}$  doped samples. This can be  
 10 reasonably interpreted. Firstly,  $\text{Cu}^{2+}$  doping promotes the oxygen surface adsorption  
 11 ability of the  $\text{PrSrCo}_{1-x}\text{Cu}_x\text{O}_{4+\delta}$  oxides (as that proved from the O1s XPS results).  
 12 Secondly, the interstitial oxygen concentration ( $\delta$ ) increases with the increase of  $\text{Cu}^{2+}$   
 13 doping concentration (table 2). Diffusion of interstitial oxygen may enhance oxygen  
 14 reduction reaction occurring on the cathode in the intermediate temperature range.  
 15 [44-47].

16 Fig. 5 shows the typical normalized conductivity relaxation transient curves for  
 17  $\text{PrSrCo}_{0.7}\text{Cu}_{0.3}\text{O}_{4+\delta}$ . The values of  $D_{\text{chem}}$  and  $k_{\text{chem}}$  are obtained from fitting the

1 normalized conductivities to the appropriate solution of Fick's second law (inset, Fig.  
 2 5). The  $D_{\text{chem}}$  and  $k_{\text{chem}}$  values obtained at 750°C in this study are  $1.39 \times 10^{-4} \text{ cm}^2 \text{ s}^{-1}$   
 3 and  $1.28 \times 10^{-2} \text{ cm s}^{-1}$  respectively. For comparison, the  $D_{\text{chem}}$  value of  $5.5 \times 10^{-4} \text{ cm}^2$   
 4  $\text{s}^{-1}$  and  $k_{\text{chem}}$  of  $2.1 \times 10^{-2} \text{ cm s}^{-1}$  at 750 °C were reported by Saher et al. for  $\text{Pr}_2\text{NiO}_{4+\delta}$   
 5 [48]. Li et al. measured a  $D_{\text{chem}}$  and  $k_{\text{chem}}$  values of  $3.5 \times 10^{-5} \text{ cm}^2 \text{ s}^{-1}$  and  $1.6 \times 10^{-3} \text{ cm}$   
 6  $\text{s}^{-1}$  at 750 °C for  $\text{La}_2\text{NiO}_{4+\delta}$  [49]. It can be seen that oxygen transport properties of  
 7  $\text{PrSrCo}_{0.7}\text{Cu}_{0.3}\text{O}_{4+\delta}$  is comparable to those cathode materials with excellent ORR  
 8 activity reported in the literatures.

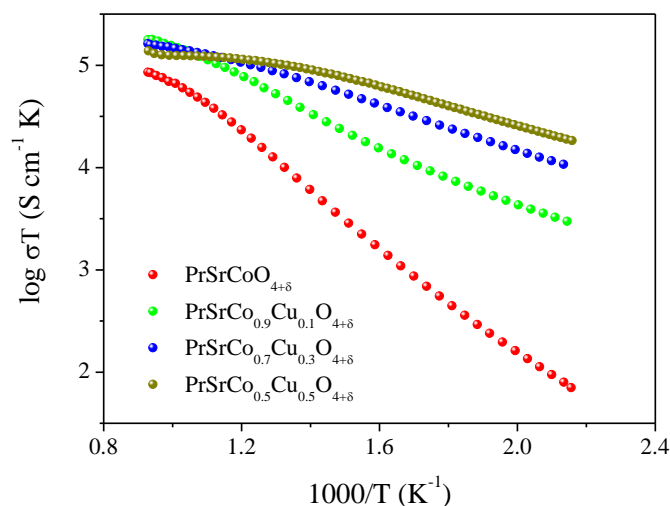


9  
 10 Fig. 5. Normalized conductivity transients measured on  $\text{PrSrCo}_{0.7}\text{Cu}_{0.3}\text{O}_{4+\delta}$  cathode  
 11 material at different temperatures.

### 12 3.4 Electrical conductivity

13 Fig. 6 presents the conductivity of  $\text{PrSrCo}_{1-x}\text{Cu}_x\text{O}_{4+\delta}$  as a function of temperature in  
 14 air. All the materials show gradual increase of the conductivity with the measuring  
 15 temperature. It is observed that the conductivity of  $\text{Cu}^{2+}$  doped materials are always  
 16 higher than  $\text{PrSrCoO}_{4+\delta}$ , and it increases further with the  $\text{Cu}^{2+}$  doping concentration.

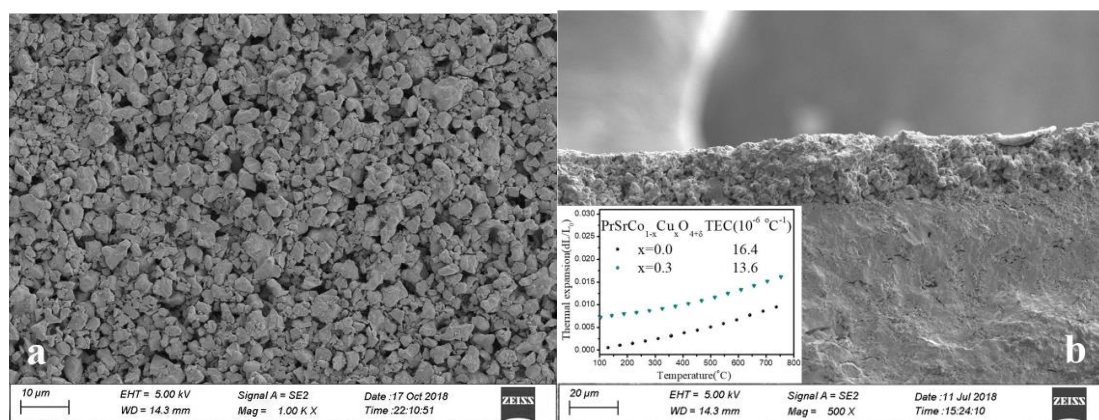
1 The conductivity values of all samples exceed  $100 \text{ S cm}^{-1}$  at  $700 \text{ }^\circ\text{C}$ , meeting the  
 2 requirement of the SOFC cathode materials.



3  
 4 Fig. 6. Temperature dependencies of electrical conductivity of  $\text{PrSrCo}_{1-x}\text{Cu}_x\text{O}_{4+\delta}$  ( $x =$   
 5  $0.0 \sim 0.5$ ) in air at different temperatures.

### 6 3.5 Electrocatalytic activity

7 In order to investigate the electrochemical properties, symmetrical cells are  
 8 constructed with  $\text{PrSrCo}_{1-x}\text{Cu}_x\text{O}_{4+\delta}$  electrode and GDC electrolyte. Fig.7 shows the  
 9 surface and cross-section SEM images of  $\text{PrSrCo}_{0.7}\text{Cu}_{0.3}\text{O}_{4+\delta}$  cathode on GDC  
 10 electrolyte that sintered at  $950 \text{ }^\circ\text{C}$  for 3 hours. Clearly  $\text{PrSrCo}_{0.7}\text{Cu}_{0.3}\text{O}_{4+\delta}$  adheres



11  
 12 Fig.7. SEM images of the  $\text{PrSrCo}_{0.7}\text{Cu}_{0.3}\text{O}_{4+\delta}$  electrode sintered at  $950 \text{ }^\circ\text{C}$  for 3 h (a):

1 surface; b: cross section).

2 tightly on the dense GDC electrolyte, to form a porous cathode with thickness  $\sim 22$

3  $\mu\text{m}$  and no obvious delamination can be observed. This result is due to the similar

4 TEC value of  $\text{PrSrCo}_{0.7}\text{Cu}_{0.3}\text{O}_{4+\delta}$  ( $13.6 \times 10^{-6} \text{ }^\circ\text{C}$ ) and GDC electrolyte ( $13.1 \times 10^{-6} \text{ }^\circ\text{C}$ )

5 (inset figure 7b). It is also observed that the TEC value has been greatly reduced in

6 the  $\text{Cu}^{2+}$  doped material.

7 Fig. 8a shows the impedance spectra of  $\text{PrSrCo}_{0.7}\text{Cu}_{0.3}\text{O}_{4+\delta}$  cathode measured at

8 different temperatures. Obviously depressed arcs with irregular shape are observed at

9 the measurement temperatures. The polarization resistance ( $R_p$ ) is obtained from the

10 difference between low frequency intersection and high frequency one with Z 'axis. It

11 is observed that  $R_p$  decreases rapidly with the increase of measurement temperature,

12 showing a thermoactivated ORR reaction. Fig. 8b shows the Arrhenius plot of  $R_p$  as a

13 function of temperature. The  $R_p$  value of 0.46, 0.14, 0.08 and 0.18  $\Omega \text{ cm}^2$  are

14 obtained at 700  $^\circ\text{C}$  for  $x = 0.0, 0.1, 0.3$  and  $0.5$ , respectively. It can be seen that  $\text{Cu}^{2+}$

15 doping significantly improves the catalytic performance of the electrode. This may be

16 because the incorporation of copper ions increases the interstitial oxygen

17 concentration in the material, which improves the oxygen ion transport performance.

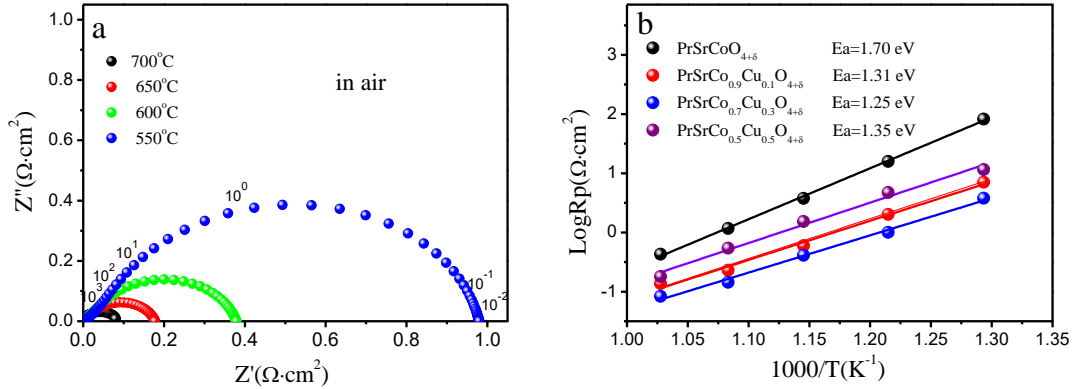
18 The activation energy of ORR is obtained from the slope of the Arrhenius plot, and

19 the results are listed in Fig. 8b. Compared to the pristine  $\text{PrSrCoO}_{4+\delta}$ , the activation

20 energy of  $\text{Cu}^{2+}$  doped cathode is significantly reduced, suggesting that the oxygen

21 reduction mechanism on the copper-doped electrode is different from that of

1 PrSrCoO<sub>4+δ</sub>.

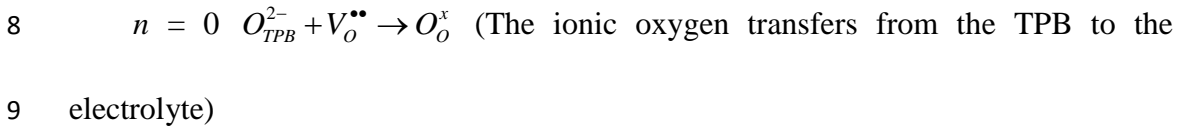
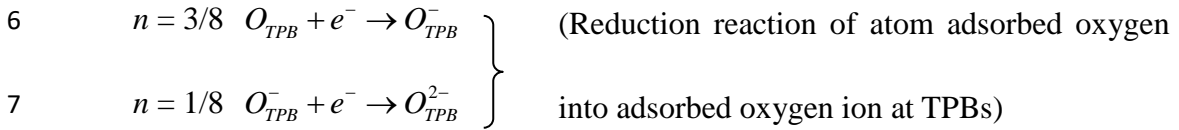
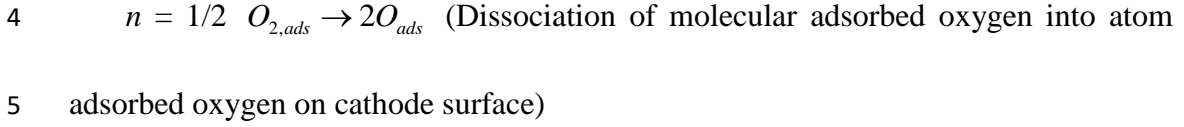


2

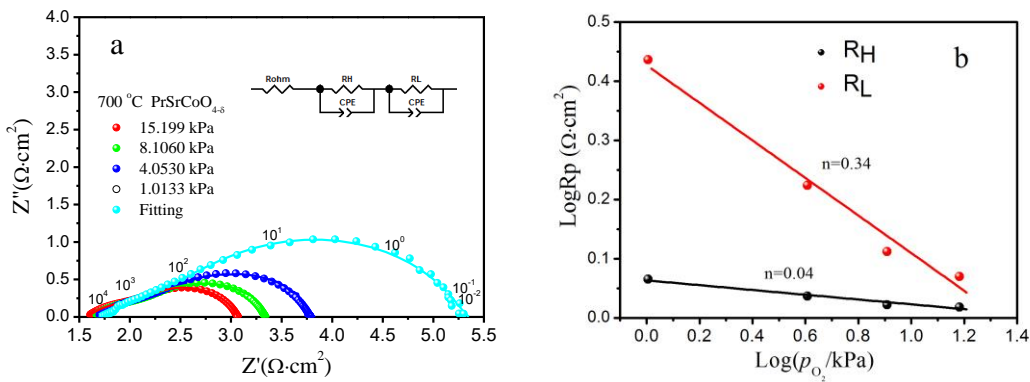
3 Fig. 8. (a) Nyquist plots of PrSrCo<sub>0.7</sub>Cu<sub>0.3</sub>O<sub>4+δ</sub> cathode measured at different  
 4 temperatures in air. In order to show clearly the change of Rp with temperature, the  
 5 resistance contribution of electrolyte and lead wires have been removed from the plot;  
 6 (b) Polarization resistance plotted versus inverse temperature for PrSrCo<sub>1-x</sub>Cu<sub>x</sub>O<sub>4+δ</sub> (x  
 7 = 0.0, 0.1, 0.3, 0.5) cathodes.

8 In order to further understand the rate control step of the oxygen reduction (ORR) on  
 9 different electrodes, the impedance spectra of PrSrCoO<sub>4+δ</sub> and PrSrCo<sub>0.7</sub>Cu<sub>0.3</sub>O<sub>4+δ</sub> are  
 10 collected at 700 °C under different oxygen partial pressures, and fitted with equivalent  
 11 circuit R<sub>ohm</sub>-(R<sub>H</sub>-CPE)-(R<sub>L</sub>-CPE) (Fig.9a and Fig.10a). Here R<sub>ohm</sub> is the resistant  
 12 contribution of GDC electrolyte and lead wires, R<sub>H</sub> and R<sub>L</sub> represent the polarization  
 13 resistances of high frequency arc and low frequency arc related electrode processes.  
 14 The electrochemical reaction mechanism on the cathode is studied by plotting R<sub>H</sub> and  
 15 R<sub>L</sub> as a function of oxygen partial pressure ( $P_{O_2}$ ), respectively (Fig.9b and Fig.10b). It  
 16 is known that the variation of Rp vs  $P_{O_2}$  can be well described by the following  
 17 expression:  $R_p = R_p^0 \times (P_{O_2})^n$

1 The  $n$  values give information about the species involved in the electrode reactions  
 2 [50-52]

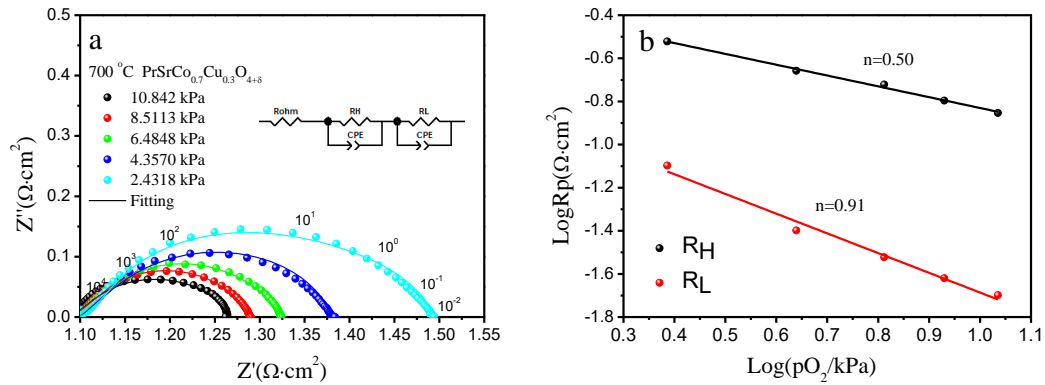


10 Obviously,  $PrSrCoO_{4+\delta}$  and  $PrSrCo_{0.7}Cu_{0.3}O_{4+\delta}$  cathodes exhibit different reaction  
 11 order ( $n$ ). For  $PrSrCoO_{4+\delta}$  cathode, the value of  $n$  is about 0.04 for  $R_H$ , which can be  
 12 ascribed to the step of oxygen ions transfer through the electrode and  
 13 electrode/electrolyte interface. The  $n$  value of low frequency arc is about 0.34, which  
 14 is close to 3/8. Therefore, the low frequency arc is confirmed to be related to the



15  
 16 Fig. 9. (a) Impedance plots of the  $PrSrCoO_{4+\delta}$  electrode with different morphologies  
 17 measured at 700 °C in air; (b) Logarithm plot of polarization resistance vs oxygen

1 partial pressure.



2

3 Fig. 10. (a) Impedance spectra for the  $\text{PrSrCo}_{0.7}\text{Cu}_{0.3}\text{O}_{4+\delta}$  cathode on GDC at 700 °C

4 under various oxygen partial pressures; (b) Logarithm plot of polarization resistance

5 vs oxygen partial pressure.

6 charge transfer process. In the whole range of the oxygen partial pressure that

7 measured, the value of  $R_L$  is always larger than that of  $R_H$ , which means that the

8 charge transfer process on  $\text{PrSrCoO}_{4+\delta}$  cathode is the rate-limiting step. In the case of

9  $\text{PrSrCo}_{0.7}\text{Cu}_{0.3}\text{O}_{4+\delta}$  cathode, however the magnitude of  $n$  for high frequency arc is

10 close to 1/2, which suggests this process relates to the dissociation of the adsorbed

11 molecular oxygen and surface diffusion. In addition, the  $n$  value of low frequency arc

12 is about 1.0, suggesting a diffusion process of gas oxygen inside the porous cathode.

13 The larger resistance value of  $R_H$  than that of  $R_L$  under various oxygen partial

14 pressures means that the reaction rate-limiting step on  $\text{PrSrCo}_{0.7}\text{Cu}_{0.3}\text{O}_{4+\delta}$  cathode is

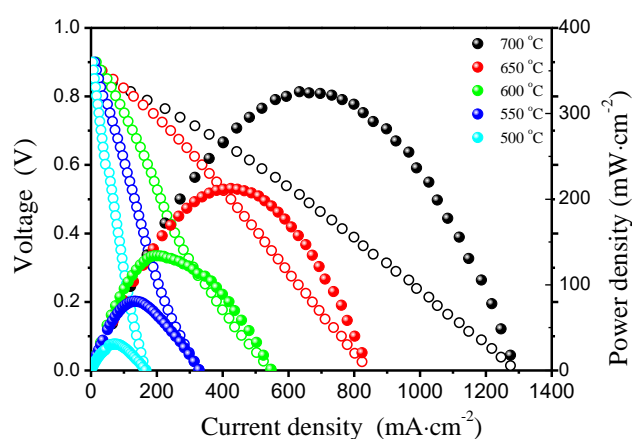
15 the dissociation and surface diffusion of the adsorbed molecular oxygen. In summary,

16 we found that  $\text{Cu}^{2+}$  doping in  $\text{PrSrCoO}_{4+\delta}$  cathode changes the oxygen reduction

17 mechanism from the charge transfer process to the dissociation of adsorbed molecular

1 oxygen and surface diffusion process.

2 Fig.11 presents the I-V and I-P curves of the electrolyte support single cell with the  
3 configuration of Ni-GDC|GDC|PrSrCo<sub>0.7</sub>Cu<sub>0.3</sub>O<sub>4+δ</sub>. The single cell exhibits the  
4 maximum power density of 327 mW cm<sup>-2</sup> at 700 °C. This value is much higher than  
5 that of 201 mW cm<sup>-2</sup> for (Pr<sub>0.9</sub>La<sub>0.1</sub>)<sub>2</sub>Ni<sub>0.74</sub>Cu<sub>0.21</sub>Ga<sub>0.05</sub>O<sub>4+δ</sub> cathode [53] and 298 mW  
6 cm<sup>-2</sup> for Pr<sub>2</sub>NiO<sub>4</sub> cathode [54] at 700 °C reported in the literatures with similar cell  
7 configuration. Accordingly, the oxygen exchange capacity and electrocatalytic  
8 performance of PrSrCoO<sub>4</sub> cathode are successfully improved by Cu<sup>2+</sup> doping strategy.  
9 PrSrCo<sub>0.7</sub>Cu<sub>0.3</sub>O<sub>4+δ</sub> is proved to be a potential cathode material for IT-SOFCs.



10

11 Fig. 11. Cell voltage and power density as a function of current density for  
12 electrolyte-supported cells Ni-GDC/GDC/ PrSrCo<sub>0.7</sub>Cu<sub>0.3</sub>O<sub>4+δ</sub> with humidified H<sub>2</sub> as  
13 fuel and ambient air as oxidant.

#### 14 4. Conclusions

15 PrSrCo<sub>1-x</sub>Cu<sub>x</sub>O<sub>4+δ</sub> ( $x = 0.0, 0.1, 0.3, 0.5$ ) materials were synthesized by solid-state  
16 reaction method. The results show that PrSrCo<sub>1-x</sub>Cu<sub>x</sub>O<sub>4+δ</sub> has good chemical and

1 thermal compatibility with GDC electrolyte. Copper doping increases the interstitial  
2 oxygen concentration and improves the electrochemical performance of the material.  
3  $\text{PrSrCo}_{0.7}\text{Cu}_{0.3}\text{O}_{4+\delta}$  cathode exhibits the lowest polarization resistance of  $0.08 \Omega \text{ cm}^2$   
4 at  $700^\circ\text{C}$ , and the rate determining step (RDS) of  $\text{PrSrCo}_{0.7}\text{Cu}_{0.3}\text{O}_{4+\delta}$  cathode is  
5 dissociation of the adsorbed molecular oxygen and surface diffusion process.

6 **Acknowledgement:**

7 The project was supported by National Natural Science Foundation of China  
8 (51872078 and 51372073).

9

## 1 **References**

- 2 [1] E. Boehm, J.M. Bassat, P. Dordor, F. Mayvy, J.C. Grenier, P. Stevens, Oxygen  
3 diffusion and transport properties in non-stoichiometric  $\text{Ln}_{2-x}\text{NiO}_{4+\delta}$  oxides, *Solid*  
4 *State Ion.* 176 (2005) 2717-2725.
- 5 [2] L.P. Sun, Q. Li, L.H. Huo, H. Zhao, G.Y. Zhang, N. Lin, J.P. Viricelle, C. Pijolat,  
6 Synthesis and performance of  $\text{Sr}_{1.5}\text{La}_x\text{MnO}_4$  as cathode materials for intermediate  
7 temperature solid oxide fuel cell, *J. Power Sources.* 196 (2011) 5835-5839.
- 8 [3] N.V. Lyskov, G.N. Mazo, L.S. Leonova, L.M. Kolchina, S.Ya. Istomin, E.V.  
9 Antipov, The effect of temperature and oxygen partial pressure on the reduction  
10 mechanism in the  $\text{Pr}_2\text{CuO}_4/\text{Ce}_{0.9}\text{Gd}_{0.1}\text{O}_{1.95}$  system, *Russ. J. Electrochem.* 49 (2013)  
11 747-752.
- 12 [4] R. Sayers, S.J. Skinner, Evidence for the catalytic oxidation of  $\text{La}_2\text{NiO}_{4+\delta}$ , *J.*  
13 *Mater. Chem. A.* 21 (2011) 414-419.
- 14 [5] S.J. Skinner, J.A. Kilner, Oxygen diffusion and surface exchange in  
15  $\text{La}_{2-x}\text{Sr}_x\text{NiO}_{4+\delta}$ , *Solid State Ion.* 135 (2000) 709-712.
- 16 [6] A. Chroneos, D. Parfitt, J.A. Kilner, R.W. Grimes, Anisotropic oxygen diffusion in  
17 tetragonal  $\text{La}_2\text{NiO}_{4+\delta}$ : molecular dynamics calculations, *J. Mater. Chem.* 20 (2010)  
18 266-270.
- 19 [7] R.K. Sharma, M. Burriel, L. Dessemond, J.M. Bassat, E. Djurado, Design of  
20 interfaces in efficient  $\text{Ln}_2\text{NiO}_{4+\delta}$  (Ln=La, Pr) cathodes for SOFC applications, *J.*  
21 *Mater. Chem. A.* 4 (2016) 12451-12462.

- 1 [8] R.K. Sharma, S.K. Cheal, M. Burriel, L. Dessemond, J.M. Bassat, E. Djurado,  
2 Design of  $\text{La}_{2-x}\text{Pr}_x\text{NiO}_{4+\delta}$  SOFC cathodes: a compromise between electrochemical  
3 performance and thermodynamic stability, *J. Mater. Chem. A*. 5 (2017) 1120-1132.
- 4 [9] T. Inprasit, S. Wongkasemjit, S.J. Skinner, M. Burrie, P. Limthongkul, Effect of Sr  
5 substituted  $\text{La}_{2-x}\text{Sr}_x\text{NiO}_{4+\delta}$  ( $x=0, 0.2, 0.4, 0.6, 0.8$ ) on oxygen stoichiometry and  
6 oxygen transport properties, *RSC Adv.* 5 (2015) 2486-2492.
- 7 [10] L.M. Kolchina, N.V. Lyskov, A.N. Kuznetsov, S.M. Kazakov, M.Z. Galin, A.  
8 Meledin, A.M. Abakumov, S.I. Bredikhin, G.N. Mazo, E.V. Antipov, Evaluation of  
9 Ce-doped  $\text{Pr}_2\text{CuO}_4$  for potential application as a cathode material for solid oxide fuel  
10 cells, *RSC Adv.* 6 (2016) 101029-101037.
- 11 [11] L.M. Kolchina, N.V. Lyskov, P.P. Pestrikov, S.Y. Istomin, G.N. Mazo, E.V.  
12 Antipov, Evaluation of  $\text{La}_{1.8-x}\text{Pr}_x\text{Sr}_{0.2}\text{CuO}_{4-\delta}$  oxides as cathode materials for IT-SOFCs,  
13 *Mater. Chem. Phys.* 165 (2015) 91-96.
- 14 [12] Y. Chen, B.M. Qian, G.M. Yang, D.J. Chen, Z.P. Shao, Insight into an unusual  
15 lanthanum effect on the oxygen reduction reaction activity of Ruddlesden- Popper-  
16 type cation-nonstoichiometric  $\text{La}_{2-x}\text{NiO}_{4+\delta}$  ( $x = 0-0.1$ ) oxides, *J. Mater. Chem. A*. 3  
17 (2015) 6501-6508.
- 18 [13] Y.N. Shen, H.L. Zhao, X.T. Liu, N.S. Xu, Preparation and electrical properties of  
19 Ca-doped  $\text{La}_2\text{NiO}_{4+\delta}$  cathode materials for IT-SOFC, *Phys. Chem. Chem. Phys.* 12  
20 (2010) 15124-15131.
- 21 [14] H. Li, Z. Cai, Q. Li, C. Sun, H. Zhao, Electrochemical investigation of

- 1 Pr<sub>2</sub>CuO<sub>4</sub>-based composite cathode for intermediate-temperature solid oxide fuel cells,  
2 J. Alloy. Compd. 688 (2016) 972-977.
- 3 [15] L.P. Sun, H. Zhao, Q. Li, L.H. Huo, J.P. Viricelle, C. Pijolat, Study of oxygen  
4 reduction mechanism on Ag modified Sm<sub>1.8</sub>Ce<sub>0.2</sub>CuO<sub>4</sub> cathode for solid oxide fuel  
5 cell, Int. J. Hydrog. Energy. 38 (2013) 14060-14066.
- 6 [16] Q. Li, H. Zhao, L.H. Huo, L.P. Sun, X.L. Cheng, J.C. Grenier, Electrode  
7 properties of Sr doped La<sub>2</sub>CuO<sub>4</sub> as new cathode material for intermediate-temperature  
8 SOFCs, Electrochem. Commun. 9 (2007) 1508-1512.
- 9 [17] L.P. Sun, Q. Li, H. Zhao, J.H. Hao, L.H. Huo, G.S. Pang, Z. Shi, S.H. Feng,  
10 Electrochemical performance of Nd<sub>1.93</sub>Sr<sub>0.07</sub>CuO<sub>4</sub> nanofiber as cathode material for  
11 SOFC, Int. J. Hydrog. Energy. 37 (2012) 11955-11962.
- 12 [18] T. Ishihara, Oxide ion conductivity in defect perovskite Pr<sub>2</sub>NiO<sub>4</sub> and its  
13 application for solid oxide fuel cells, J. Ceram. Soc. Jpn. 122 (2014) 179-186.
- 14 [19] T. Zhao, L.P. Sun, Q. Li, L.H. Huo, H. Zhao, J.M. Bassat, A. Rougier, S.  
15 Fourcade, J.C. Grenier, Electrochemical property assessment of Pr<sub>2</sub>CuO<sub>4</sub>  
16 submicrofiber cathode for intermediate-temperature solid oxide fuel cells, J.  
17 Electrochem. Energy Convers. Storage. 13 (2016) 011006.
- 18 [20] C. Sun, Q. Li, L.P. Sun, H. Zhao, L.H. Huo, Characterization and electrochemical  
19 performances of Pr<sub>2</sub>CuO<sub>4</sub> as a cathode material for intermediate temperature solid  
20 oxide fuel cells, Mater. Res. Bull. 53 (2014) 65-69.
- 21 [21] C. Munning, S. Skinner, G. Amow, P. Whitfield, I. Davidson, Oxygen transport in

- 1 the LaNiCoO<sub>4</sub> system, Solid State Ion. 176 (2005) 1895-1901.
- 2 [22] Y.S. Wang, H.W. Nie, S.R. Wang, T.L. Wen, U. Guth, V. Valshook,  
3 A<sub>2-α</sub>A<sub>α</sub>'BO<sub>4</sub>-type oxides as cathode materials for IT-SOFCs (A = Pr, Sm; A' = Sr; B  
4 = Fe, Co), Mater. Lett. 60 (2006) 1174-1178.
- 5 [23] C. Tealdi, C. Ferrara, P. Mustarelli, M. Saiful Islam, Vacancy and interstitial  
6 oxide ion migration in heavily doped La<sub>2-x</sub>Sr<sub>x</sub>CoO<sub>4±δ</sub>, J. Mater. Chem. A. 22 (2012)  
7 8969-8975.
- 8 [24] J.K. Wang, J. Zhou, W.W. Fan, W.D. Wang, K. Wu, Y.H. Cheng, Investigation of  
9 structural and electrochemical properties of LaSrCo<sub>1-x</sub>Sb<sub>x</sub>O<sub>4</sub> (0≤X≤0.20) as potential  
10 cathode materials in intermediate-temperature solid oxide fuel cells, J. Solid State  
11 Chem. 247 (2017) 24-30.
- 12 [25] Y. Cao, H.T. Gu, H. Chen, Y.F. Zheng, M. Zhou, L.C. Guo, Preparation and  
13 characterization of Pr<sub>2-x</sub>Sr<sub>x</sub>CoO<sub>4+δ</sub> cathode materials for IT-SOFC, J. Inorg. Mater.  
14 25 (2010) 738-742.
- 15 [26] L. Gao, M.Z. Zhu, Q. Li, L.P. Sun, H. Zhao, J.C. Grenier, Electrode properties of  
16 Cu-doped Bi<sub>0.5</sub>Sr<sub>0.5</sub>FeO<sub>3-δ</sub> cobalt-free perovskite as cathode for intermediate-  
17 temperature solid oxide fuel cells, J. Alloy. compd. 700 (2017) 29-36.
- 18 [27] Q. Li, T. Xia, L.P. Sun, H. Zhao, L.H. Huo, Electrochemical performance of  
19 novel cobalt-free perovskite SrFe<sub>0.7</sub>Cu<sub>0.3</sub>O<sub>3-δ</sub> cathode for intermediate temperature  
20 solid oxide fuel cells, Electrochim. Acta. 150 (2014) 151-156.
- 21 [28] G.N. Mazo, S.M. Kazakov, L.M. Kolchina, A.V. Morozov, S.Y. Istomin, NV.

- 1 Lyskov, A.A. Gippius, E.V. Antipov, Thermal expansion behavior and high-  
2 temperature electrical conductivity of  $A_{2-x}A'_x\text{Cu}_{1-y}\text{Co}_y\text{O}_{4\pm\delta}$  ( $A=\text{La, Pr}$ ;  $A'=\text{Pr, Sr}$ )  
3 oxides with the  $\text{K}_2\text{NiF}_4$ -type structure, *J. Alloy. Compd.* 639 (2015) 381-386.
- 4 [29] N.V. Lyskov, M.S. Kaluzhskikh, L.S. Leonova, G.N. Mazo, S.Y. Istomin, E.V.  
5 Antipov, Electrochemical characterization of  $\text{Pr}_2\text{CuO}_4$  cathode for IT-SOFC, *Int. J.*  
6 *Hydrog. Energy.* 37 (2012) 18357-18364.
- 7 [30] K. Zheng, A. Gorzkowska-sobaś, K. Świerczek, Evaluation of  $\text{Ln}_2\text{CuO}_4$  ( $\text{Ln: La,}$   
8  $\text{Pr, Nd}$ ) oxides as cathode materials for IT-SOFCs, *Mater. Res. Bull.* 47 (2012)  
9 4089-4095.
- 10 [31] A. Hassen, A.I. Ali, B.G. Kim, A. Krimmel, Structure-Property Relationships in  
11  $\text{Pr}_{1-x}\text{Sr}_{1+x}\text{CoO}_4$  ( $0 \leq x \leq 0.40$ ), *Am. J. Condensed Matter Physics.* 2 (2012) 93-100.
- 12 [32] T. Nakamura, Y. Ling, K. Amezawa, The effect of interstitial oxygen formation  
13 on the crystal lattice deformation in layered perovskite oxides for electrochemical  
14 devices, *J. Mater. Chem. A.* 3 (2015) 10471-10479.
- 15 [33] A.R. Gilev, E.A. Kiselev, D.M. Zakharov, V.A. Cherepanov, Effect of calcium  
16 and copper/iron co-doping on defect-induced properties of  $\text{La}_2\text{NiO}_4$ -based materials, *J.*  
17 *Alloy. Compd.* 753 (2018) 491-501.
- 18 [34] A. Aguadero, J.A. Alonso, M.J. Escudero, L. Daza, Evaluation of the  
19  $\text{La}_2\text{Ni}_{1-x}\text{Cu}_x\text{O}_{4+\delta}$  system as SOFC cathode material with 8YSZ and LSGM as  
20 electrolytes, *Solid State Ion.* 179 (2008) 393–400
- 21 [35] A.P. Tarutin, J.G. Lyagaeva, A.S. Farlenkov, A.I. Vylkov, D.M. Medvedev,

- 1 Cu-substituted  $\text{La}_2\text{NiO}_{4+\delta}$  as oxygen electrodes for protonic ceramic electrochemical  
2 cells, *Ceram. Int.* 45 (2019) 16105–16112
- 3 [36] L. Jiang, T. Wei, R. Zeng, W.X. Zhang, Y.H. Huang, Thermal and  
4 electrochemical properties of  $\text{PrBa}_{0.5}\text{Sr}_{0.5}\text{Co}_{2-x}\text{Fe}_x\text{O}_{5+\delta}$  ( $x=0.5, 1.0, 1.5$ ) cathode  
5 materials for solid oxide fuel cells, *J. Power Sources.* 232 (2013) 279-285.
- 6 [37] F.J. Jin, H.W. Xu, W. Long, Y. Shen, T.M. He, Characterization and evaluation of  
7 double perovskites  $\text{LnBaCoFeO}_{5+\delta}$  ( $\text{Ln}=\text{Pr}$  and  $\text{Nd}$ ) as intermediate-temperature solid  
8 oxide fuel cell cathodes, *J. Power Sources.* 243 (2013) 10-18.
- 9 [38] T. Chen, S.L. Pang, X.Q. Shen, X.N. Jiang, W.Z. Wang, Evaluation of  
10 Ba-deficient  $\text{PrBa}_{1-x}\text{Fe}_2\text{O}_{5+\delta}$  oxides as cathode materials for intermediate-temperature  
11 solid oxide fuel cells, *RSC Adv.* 6(2016) 13829-13836
- 12 [39] Z.Z. Chen, J.L. Wang, D.M. Huan, S.J. Sun, G.P. Wang, Z.P. Fu, W.H. Zhang, Z.S.  
13 Zheng, H.B. Pan, R.R. Peng, Y.L. Lu, Tailoring the activity via cobalt doping of a  
14 two-layer Ruddlesden-Popper phase cathode for intermediate temperature solid oxide  
15 fuel cells, *J. Power Sources.* 371(2017) 41-47.
- 16 [40] E.Y. Konyshcheva, M.V. Kuznetsov, Fluctuation of surface composition and  
17 chemical states at hetero-interface in composites comprised of a phase with perovskite  
18 structure and a phase related to the Ruddlesden-Popper family of compounds, *RSC*  
19 *Adv.* 3 (2013) 14114-14122.
- 20 [41] J.H. Kim, X-ray photoelectron spectroscopy analysis of  $(\text{Ln}_{1-x}\text{Sr}_x)\text{CoO}_{3-\delta}$  ( $\text{Ln}$ : Pr,  
21 Nd and Sm), *Appl. Surf. Sci.* 258 (2011) 350-355.

- 1 [42] M.I. Ivanovskaya, D.A. Kotikov, V.V. Pan'kov, V.V. Zyryanov, Structure of  
2 SrCo<sub>0.5</sub>Fe<sub>0.5</sub>O<sub>3-δ</sub>-based composites prepared by sol-gel and mechanochemical  
3 processes, *Inorg. Mater.* 45 (2009) 910-915.
- 4 [43] Y.Q. Meng, L. Sun, J. Gao, W.Z. Tan, C.S. Chen, J.X. Yi, H.J.M. Bouwmeester,  
5 Z.H. Sun, K.S. Brinkman, Insights into the CO<sub>2</sub> stability-performance trade-off of  
6 antimony-doped SrFeO<sub>3-δ</sub> perovskite cathode for solid oxide fuel cells, *ACS. Appl.*  
7 *Mater. Interfaces.* 11(2019) 11498-11506.
- 8 [44] S. Takahashi, S. Nishimoto, M. Matsuda, M. Miyake, Electrode properties of the  
9 Ruddlesden-Popper series, La<sub>n+1</sub>Ni<sub>n</sub>O<sub>3n+1</sub> (n=1, 2, 3), as intermediate-temperature  
10 solid oxide fuel cells, *J. Am. Ceram. Soc.* 93 (2010) 2329-2333.
- 11 [45] F. Manvy, C. Lalanne, J.M. Bassat, J.C. Grenier, H. Zhao, P. Dordor, P. Stevens,  
12 Oxygen reduction on porous Ln<sub>2</sub>NiO<sub>4+δ</sub> electrodes, *J. Eur. Ceram. Soc.* 25(2005)  
13 2669-2672.
- 14 [46] K. Kammer, An EIS study of La<sub>2-x</sub>Sr<sub>x</sub>NiO<sub>4+δ</sub> SOFC cathode, *Ionics* 15(2009)  
15 325-328.
- 16 [47] C. Lalanne, F. Mauvy, E. Siebert, M.L. Fontaine, J.M. Bassat, F. Ansart, P.  
17 Stevens, J.C. Grenier, Intermediate temperature SOFC single cell test using  
18 Nd<sub>1.95</sub>NiO<sub>4+δ</sub> as cathode, *J. Eur. Ceram. Soc.* 27(2007) 4195-4198.
- 19 [48] S. Saher, J. Song, V. Vibhu, C. Nicollet, A. Flura, J.M. Bassat, H.J.M.  
20 Bouwmeester, Influence of annealing at intermediate temperature on oxygen transport  
21 kinetics of Pr<sub>2</sub>NiO<sub>4+δ</sub>, *J. Mater. Chem. A.* 6 (2018) 8331-8339.

- 1 [49] Z.A. Li, R. Haugrud, Effects of surface coatings on the determination of  $D_{\text{chem}}$   
2 and  $k_{\text{chem}}$  in  $\text{La}_2\text{NiO}_{4+\delta}$  by conductivity relaxation, *Solid State Ion.* 206 (2012) 67-71.
- 3 [50] A.P. Khandale, M.G. Bansod, S.S. Bhoga, Improved electrical and  
4 electrochemical performance of co-doped  $\text{Nd}_{1.8}\text{Sr}_{0.2}\text{Ni}_{1-x}\text{Cu}_x\text{O}_{4+\delta}$ , *Solid State Ion.*  
5 276 (2015) 127-135.
- 6 [51] Z. Gao, X.M. Liu, B. Bergman, Z. Zhao, Investigation of oxygen reduction  
7 reaction kinetics on  $\text{Sm}_{0.5}\text{Sr}_{0.5}\text{CoO}_{3-\delta}$  supported on  $\text{Ce}_{0.85}\text{Sm}_{0.075}\text{Nd}_{0.075}\text{O}_{2-\delta}$  electrolyte,  
8 *J. Power Sources.* 196 (2011) 9195-9203.
- 9 [52] J.D. Kim, G.D. Kim, J.W. Moon, Y.I. Park, W.H. Lee, K. Kobayashi, M. Nagai,  
10 C.E. Kim, Characterization of LSM-YSZ composite electrode by ac impedance  
11 spectroscopy, *Solid State Ion.* 143 (2001) 379-389.
- 12 [53] Y.X. Wang, X.Y. Zhao, S.Q. Lü, B. Yu, X.W. Meng, Y.J. Zhang, J.H. Yang, C.W.  
13 Fu, Y. Ji,  $(\text{Pr}_{0.9}\text{La}_{0.1})_2\text{Ni}_{0.74}\text{Cu}_{0.21}\text{Ga}_{0.05}\text{O}_{4+\delta}$  as cathode material for  $\text{CeO}_2$ -based  
14 intermediate-temperature solid-oxide fuel cell, *Ceram. Int.* 40 (2014) 7321-7327.
- 15 [54] J.F. Yang, J.G. Cheng, Q.M. Jiang, Y.F. Wang, R. Wang, J.F. Gao, Preparation and  
16 electrochemical properties of strontium doped  $\text{Pr}_2\text{NiO}_4$  cathode materials for  
17 intermediate-temperature solid-oxide fuel cells, *Int. J. Hydrog. Energy.* 37 (2012)  
18 1746-1751.